Theor. Comput. Fluid Dyn. (2006) 20(1): 23–40
DOI 10.1007/s00162-005-0005-7

ORIGINAL ARTICLE

Christophe Bogey · Christophe Bailly

Investigation of downstream and sideline subsonic jet noise using Large Eddy Simulation

Received: 19 January 2005 /Accepted: 15 September 2005 / Published online: 27 January 2006

Abstract The sound fields radiated by Mach number 0.6 and 0.9, circular jets with Reynolds numbers varying from 1.7×10^3 to 4×10^5 are investigated using Large Eddy Simulations. As the Reynolds number decreases, the properties of the sound radiation do not change significantly in the downstream direction, whereas they are modified in the sideline direction. At low Reynolds numbers, for large angles downstream from the jet axis, the acoustic levels are indeed remarkably lower and a large high-frequency part of the sound spectra vanishes. For all Reynolds numbers, the downstream and the sideline sound spectra both appear to scale in frequency with the Strouhal number. However their peak amplitudes vary following two different velocity exponents according to the radiation direction. The present observations suggest the presence of two sound sources: a Reynolds number-dependent source, predominant for large radiation angles, connected to the randomly-developing turbulence, and a deterministic source, radiating downstream, related to a mechanism intrinsic to the jet geometry, which is still to be comprehensively described. This view agrees well with the experimental results displaying two distinguishable components in turbulent mixing noise [1, 2].

Keywords Aeroacoustics · Jets · Large Eddy Simulation

PACS 47.27.Eq · 47.27.Sd · 47.27.Wg

List of symbols

c_0	Sound velocity in the ambient medium (m/s)
d	Distance from the end of the potential core (m)
f	Frequency (Hz)
k	Wave number (1/m)
p'	Fluctuating pressure (Pa)
r_0	Jet radius (m)
u_c	Centerline mean axial velocity (m/s)
u_j	Jet velocity (m/s)
x_c	Axial location of the end of the potential core (m)
x, r, ϕ	Cylindrical coordinates (m, rad)
x, y, z	Cartesian coordinates (m)
A	Attenuation of sound by viscosity and thermal conductivity (dB)
D	Jet diameter (m)
H	Helmholtz number

Communicated by T. Colonius

C. Bogey (✉) · C. Bailly
Laboratoire de Mécanique des Fluides et d'Acoustique, UMR CNRS 5509, Ecole Centrale de Lyon, 69134 Ecully, France
E-mail: {christophe.bogey, christophe.bailly}@ec-lyon.fr

M	Jet Mach number
Mc	Source convection Mach number
Re_D	Jet Reynolds number
R_{pp}	Azimuthal correlation function of the fluctuating pressure
St	Strouhal number
T	Simulation time (s)
T_{ac}	Total time of the acoustic signals (s)
δ_θ	Shear-layer initial momentum thickness (m)
ν	Kinematic molecular viscosity (m^2/s)
ρ_j	Inflow jet centerline density (kg/m^3)
θ	Angle from the jet axis (rad)
$\lvert\boldsymbol{\omega}\rvert$	Vorticity norm (1/s)

Subscripts

$\cdot_D$	Quantity related to the downstream observation point
$\cdot_S$	Quantity related to the sideline observation point
$\cdot_{\mathrm{peak}}$	Peak value

1 Introduction

The present paper is an effort to give new insights into subsonic jet noise using numerical simulations. Indeed, after over fifty years of research, whereas in supersonic jets certain sound generation mechanisms such as the so-called Mach wave radiation have been well characterized [3], the sound sources in subsonic jets are still to be clearly identified [4]. Two conflicting theories of jet noise have for instance been proposed by researchers. In the classical theory derived from acoustic analogies, the noise radiated by subsonic jets is generated by the developing turbulence and results from the complex combination of convective amplification and acoustic-meanflow interaction [5]. In the second theory, subsonic jet noise is regarded as composed of two distinguishable components [1]: one from the large structures and/or instability waves, dominating in the downstream direction, the other from the fine-scale turbulence, dominating in the sideline direction. The presence of these two components is supported by the works of Tam *et al.* [2, 4] and Viswanathan [6, 7] who identified two independent self-similar spectra from a large experimental database of sound spectra. That of a sound source connected to the growing and decaying instability waves is also suggested by analytical works [8, 9]. This view of two noise components is attractive, but it suffers from the confusing data available in the literature, whose trends can vary between different experiments because of acoustic contamination [10] or of the use of one-third octave spectra [11]. Considering these difficulties, numerical simulations now offer an interesting tool for characterizing the properties of the jet sound field accurately, with the final aim of advancing the understanding of jet noise.

An important point to address in the study of jet noise is that of the modifications of sound pressure spectra when jet parameters such as the acoustic Mach number $\mathrm{M} = u_j/c_0$ and the Reynolds number $\mathrm{Re}_D = u_j D/\nu$ are changed (u_j is the jet exit velocity, c_0 the speed of sound in the ambient medium, D the jet diameter, and ν the kinematic molecular viscosity). There is for instance an ongoing discussion about the scaling of the peak frequencies as the jet velocity varies. At high Reynolds numbers ($\mathrm{Re}_D \geq \mathrm{Re}_D^*$ with $10^5 \leq \mathrm{Re}_D^* \leq 4 \times 10^5$ according to different authors [7, 11, 12]), at $\theta = 90^\mathrm{o}$ to the jet axis, a Strouhal number $\mathrm{St} = fD/u_j$ scaling was found both from narrow-band spectra [1] and from one-third octave spectra [13, 14, 15] (f is the frequency). For small angles, a Strouhal scaling was observed from the narrow-band spectra but an Helmholtz number $\mathrm{H} = fD/c_0$ scaling appeared from the one-third octave spectra. Zaman and Yu [11] demonstrated later that this Helmholtz scaling is an artifact of the use of one-third octaves, resulting in a shift of the peak frequency. They noted for instance that the one-third octave spectra of Lush [13] and Tanna [15], which show a constant Helmholtz number for the peak, exhibit equally well Strouhal scaling when the corresponding narrow-band spectra are considered. They also found that the best scaling for small angles is obtained with the Helmholtz number times a Doppler factor, *i.e.* with $\mathrm{H} \times (1 - 0.5\mathrm{M}\cos\theta)$. The preceding observations, made at high Reynolds numbers, are likely not to apply at low Reynolds numbers. Jet noise sources indeed appear to be modified below $\mathrm{Re}_D \simeq 10^5$, as noticed by Crighton [12] from the noise radiated by excited jets. At low Reynolds numbers ($\mathrm{Re}_D \leq \mathrm{Re}_D^*$), the properties of jet noise also change significantly [7, 16, 17], with much narrower spectra and lower pressure levels at large observation angles. Long and Arndt [17] moreover

observed experimentally an Helmholtz scaling for the peak frequencies at all radiation angles. Note that the study of low Reynolds number jets can be particularly useful for the investigation of the sound sources attributed to the coherent turbulent structures, since the range of turbulent scales is reduced by molecular viscosity as the Reynolds number decreases. Experiments at low Reynolds numbers permitted for instance a clear identification of noise generation by instabilities in supersonic jets [18]. Simulations of subsonic jets at low Reynolds numbers have also allowed to investigate sound sources using Lighthill's theory [19], and to connect the downstream sound radiation to the periodic intrusion of vortical structures into the potential core [20].

In the present work, Large Eddy Simulations (LES) of circular jets at Mach numbers M = 0.6 and 0.9, with Reynolds numbers Re_D varying from 1700 up to 4×10^5 are performed to compare their respective acoustic radiations, and thus to shed light on the sound sources. The jet initial conditions (shear-layer thickness, inflow forcing) are identical except for the diameter and the jet exit velocity, with the aim of showing the influence of the Mach and Reynolds numbers on the radiated noise in the absence of other initial-condition effects. This work is the continuation of earlier studies where Mach M = 0.9 jets at Reynolds number $\mathrm{Re}_D = 4\times10^5$ were simulated. In these studies, flow and sound properties in agreement with what is observed experimentally at high Re_D were obtained [21]. The influence of the inflow conditions [22] and of the subgrid modelling [23] on results was also investigated. It should be noted that, unlike Direct Numerical Simulation (DNS), LES can be applied to flows at any Reynolds number provided that the effective Reynolds number of the computed flows is not artificially decreased by the LES methodology, nor by the use of an overly coarse grid, and corresponds to the value given by the initial conditions. The present simulations are therefore performed using a solver especially developed for direct noise computations, with low-dissipative and low-dispersive numerical schemes [24], following an LES approach based on an explicit selective filtering instead of a classical eddy-viscosity model for subgrid modelling [21, 25]. For all the simulated jets, the properties of the sound pressure field are calculated at two observation points in the near acoustic field. These two points define angles from the jet axis, relative to an origin at the end of the jet potential core, of $\theta \simeq 30^o$ and $\theta \simeq 90^o$, respectively. The effects of the Mach and Reynolds numbers on the downstream and sideline acoustic radiations are thus investigated, in order to show evidence of two noise sources. Attention is especially drawn to the shapes of the sound spectra, to the scaling of the peak frequencies and levels, and to the azimuthal cross-correlations of the radiated pressure.

This paper is organized as follows. In Sect. 2, the main features of the numerical procedure are presented, the parameters of the different simulations are given, and the observation points are defined. The sound pressure fields radiated by the simulated jets are investigated in Sect. 3: snapshots of vorticity and pressure are shown, and the properties of the sound fields in the downstream and sideline directions are compared. The characteristics of the jet noise sources are discussed in the light of the numerical results in Sect. 4. Concluding remarks are drawn in Sect. 5.

2 Simulation parameters

2.1 Numerical procedure

The numerical algorithm is identical to that of the earlier simulation [21] of a Mach M = 0.9, Reynolds $\mathrm{Re}_D = 4\times10^5$ jet. The Cartesian filtered compressible Navier-Stokes equations are solved using numerical schemes with low dispersion and low dissipation properties [24]. A thirteen-point finite-difference scheme is used for spatial discretization, and an explicit six-stage Runge-Kutta algorithm is applied for time integration. Grid-to-grid oscillations are removed by an explicit filtering which is optimized to damp only the short waves discretized by less than four points per wavelength. This filtering is used to ensure numerical stability, and also to take into account the effects of the subgrid energy-dissipating scales without affecting the resolved scales. This approach was developed to preserve the effective Reynolds number of the jet, which might not be possible using eddy-viscosity subgrid models such as the dynamical Smagorinsky model [23]. Furthermore, in order to compute the radiated noise directly, non-reflective boundary conditions are implemented, with the addition of a sponge zone in the jet at the outflow [26].

The numerical parameters of the present simulations are those of the simulation referred to as LESac or LESsf in earlier papers [21, 22, 23]. The computational domain is discretized by a 12.5 million point Cartesian grid with 15 points within the range $0 \le r \le r_0$, and extends radially up to $r = 15r_0$ from the jet axis. Due to stretching of the axial mesh size for $x \ge 26r_0$, the turbulent flow is computed accurately up to a distance of $x = 25r_0$, and the sound field is resolved for Strouhal numbers $\mathrm{St} = fD/u_j < 2$ up to $x = 30r_0$. Finally, the

Table 1 Mach and Reynolds numbers of the simulated jets

	M	Re_D
LESm09hre	0.9	4×10^5
LESm09re10^4	0.9	10^4
LESm09re5000	0.9	5×10^3
LESm09re2500	0.9	2.5×10^3
LESm09re1700	0.9	1.7×10^3
LESm06hre	0.6	2.7×10^5
LESm06re3300	0.6	3.3×10^3
LESm06re1700	0.6	1.7×10^3

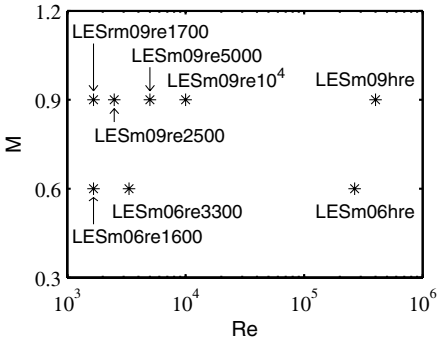

Fig. 1 Graph of the initial conditions of the simulated jets

simulation times T are long enough to achieve the convergence of statistics, as indicated for instance by the corresponding Strouhal number $D/(Tu_j) = 10^{-3}$.

For the study of the acoustic field, the spectra are computed from pressure signals of total time T_{ac} such as $D/(T_{ac}u_j) = 1.2 \times 10^{-3}$ in term of minimal Strouhal number. These signals are filtered using moving averaging in order to remove the low-frequency components with St < 0.05. They are divided into 199 overlapping sections of time $T_{ac}/100$, windowed by a Hanning function. Moreover, for the calculation of the azimuthal cross-correlations and for averaging the sound spectra. pressure is specifically recorded at two observation locations defined by the cylindrical coordinates ($x_D = 29r_0$, $r_D = 12r_0$) and ($x_S = 11r_0$, $r_S = 15r_0$), as discussed in Sect. 2.3. For both locations, pressure is considered at 31 points equally spaced azimuthally on half a circle. It is interpolated from the Cartesian grid pressure using Lagrangian polynomials.

2.2 Definition of the simulations

Eight isothermal round jets are simulated. Their initial conditions (shear-layer thickness, inflow forcing) are identical except for the diameter and the jet exit velocity, yielding Mach numbers M of 0.6 and 0.9 and Reynolds numbers Re_D varying from 1700 up to 4×10^5, as presented in Table 1 and in Fig. 1. The LESm09hre simulation is the jet simulation at Mach M = 0.9 and at the high Reynolds number $\mathrm{Re}_D = 4\times10^5$ also referred to as LESac [21, 22] or as LESsf [23] in earlier papers. In the LESm09re10^4, LESm09re5000, LESm09re2500 and LESm09re1700 simulations, the Mach number of M = 0.9 is maintained but the Reynolds number is progressively decreased down to a value of $\mathrm{Re}_D = 1700$. In the LESm06hre, LESm06re3300 and LESm06re1700 simulations, the Mach number is only M = 0.6, the first simulation is at a high Reynolds number $\mathrm{Re}_D \geq 10^5$ whereas the two others are at lower Reynolds numbers. Note also that the LESm09re1700 and the LESm06re1700 simulations are both at $\mathrm{Re}_D = 1700$.

In jet experiments, the properties of the boundary layers at the nozzle exit have been shown to depend on the Reynolds number [27]. The boundary layers are in particular thinner as the Reynolds number increases. For instance, at $\mathrm{Re}_D \geq 10^5$, a momentum thickness of the order of $10^{-3}D$ is measured, which is very thin and cannot be taken into account numerically using current computing facilities. In the present simulations, the jet nozzle is therefore not discretized. The jet inflow conditions are modeled by imposing mean flow profiles

while using a random excitation to seed the turbulence. The possible sound sources located near the nozzle exit are consequently lacking. However, as shown by near-field pressure measurements [28, 29], these sources generate high-frequency noise (typically at St $\geq$ 2). They are thus expected not to contribute significantly to the range of noise spectra, St $<$ 2, calculated in the present simulations, where the predominant components of jet noise are observed.

In all simulations, the inflow modelling parameters (shear-layer thickness, forcing) are identical. They are those specified for the LESm09hre simulation [21, 22]. Mean profiles of velocities, pressure and density are imposed at the jet inflow boundary. The axial velocity is given by a hyperbolic-tangent profile describing an annular shear layer of radius r_0 and of momentum thickness δ_θ, with a ratio $\delta_\theta/r_0 = 0.05$. Radial and azimuthal velocities are set to zero, pressure is set to the ambient pressure, and the mean density profile is obtained from the velocity profile using a Crocco-Busemann relation for an isothermal jet [21]. To trip the turbulent transition, small random disturbances are added to the velocity profiles in the shear layer zone. Finally note that the influence of the present inflow conditions and forcing on the jet flow and sound fields was studied in detail in a recent paper [22].

2.3 Definition of the observation points

To study the acoustic field radiated by the jets, pressure is recorded at points along the line defined by $y = 15r_0$ and $z = 0$, and on two half-circles at the locations denoted D and S, defined by ($x_D = 29r_0$, $r_D = 12r_0$) and ($x_S = 11r_0$, $r_S = 15r_0$). The observation points D and S are represented in the snapshot of vorticity and pressure of Fig. 2. They define angles from the jet axis, relative to an origin at the end of the jet potential core, of $\theta_D \simeq 30^o$ and $\theta_S \simeq 90^o$, respectively. In order to investigate the two jet noise components, observed respectively in the downstream and in the sideline directions, the sound properties (pressure spectra, azimuthal cross-correlations) are therefore calculated at these two points for all the simulations.

In the present work, the observation points are not located in the far acoustic field where jet noise studies are usually conducted, and the acoustic pressure at these points might be contaminated by the aerodynamic pressure. Arndt *et al.* [30] indeed showed that the pressure signal measured at the outer edge of a jet mixing layer, typically at $r = D$, is aerodynamic in nature. The magnitude of the aerodynamic pressure however decreases rapidly with the radial distance from the jet axis. Measurements of near-field pressure reported in the literature [28, 29] for Mach 0.5 and 0.85 jets suggest for instance that aerodynamic pressure is not predominant at $r = 15r_0$, for $x \leq 30r_0$. Arndt *et al.* [30] also noticed that the near-field pressure fluctuations are acoustic for wave numbers $kr > 2.0$. For $r = 15r_0$, this condition yields St $>$ 0.047 for the Mach 0.9 jet, and St $>$ 0.070 for the Mach 0.6 jet. In the present study, the dominant part of the sound pressure spectra is obtained for St $>$ 0.1. It is therefore not appreciably affected by aerodynamic disturbances. Moreover, since the pressure signals are filtered to remove the components with St $<$ 0.05, a possible low-frequency contribution of the aerodynamic pressure is noticeably minimized.

In what follows, with one exception in Fig. 13(b), Mach and Reynolds number effects on the noise radiated by the simulated jets are investigated by comparing the sound field properties obtained at the downstream and

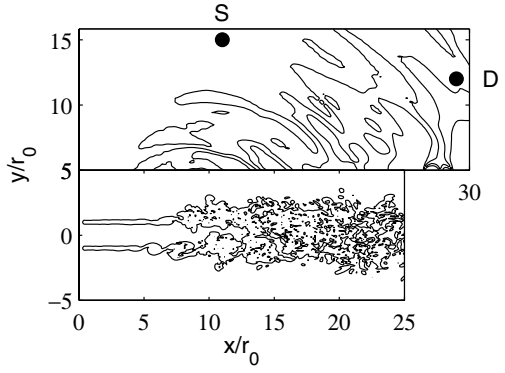

Fig. 2 Visualization of the downstream and sideline observation points D and S. Representation of the vorticity contour $|\boldsymbol{\omega}| \times r_0/u_j = 1$, and of the fluctuating pressure contours $p' = [-120, -40, 40, 120]$ Pa or $p'/(\rho_j u_j^2) = [-10.6, -3.5, 3.5, 10.6] \times 10^{-4}$ for the simulation LESm09re5000

Table 2 Jets at Mach 0.9 (top) and at Mach 0.6 (bottom): x_c is the core length; d_D and d_S are the distances, and θ_D and θ_S the angles with respect to the downstream direction, from the end of the potential core to the observation points D and S located at $(x_D = 29r_0, r_D = 12r_0)$ and $(x_S = 11r_0, r_S = 15r_0)$

	x_c/r_0	d_D/r_0	θ_D	d_S/r_0	θ_S
LESm09hre	10.2	22.3	32.6°	15	87°
LESm09re10^4	10.7	21.9	33.3°	15	88.9°
LESm09re5000	11.3	21.4	34.1°	15	91.1°
LESm09re2500	13	20	36.9°	15.1	97.6°
LESm09re1700	15.9	17.8	42.5°	15.8	108.1°
LESm06hre	9.5	22.9	31.6°	15.1	84.3°
LESm06re3300	10.7	21.9	33.3°	15	88.9°
LESm06re1700	13.3	19.8	37.4°	15.8	98.7°

the sideline observation points D and S. However, as shown in Table 2, the length of the potential core x_c is not constant in the different simulations. Consequently the distance of propagation from the sound sources to the observation points, as well as the emission angle, may vary. To check this point, the distances d_D and d_S between the end of the potentiel core, where the dominant sound sources are likely to be found, and the observation points, and the corresponding angles θ_D and θ_S with respect to the downstream direction, are provided in Table 2 for the computed jets.

For the jets at Reynolds numbers $\mathrm{Re}_D \geq 3300$ (LESm09hre, LESm09re10000, LESm09re5000, LESm06hre and LESm06re3300), the lengths of the potential core do not vary much. They are within the range $9.5r_0 \leq x_c \leq 11.3r_0$. The propagation distances and the emission angles are therefore practically constant, with $d_D \simeq 22r_0$ and $\theta_D \simeq 33°$ for the downstream point, and $d_S \simeq 15r_0$ and $\theta_S \simeq 88°$ for the sideline point. At both observation points, the differences between the sound field properties of these jets thus result only from the variations in Reynolds and Mach numbers. In other words, Reynolds and Mach effects on jet noise can be investigated qualitatively as well as quantitatively from the observation points D and S for these simulations.

For the jets at lower Reynolds numbers (LESm09re2500, LESm09re1700, LESm06re1700), the length of the potential core increases appreciably. Relative to the downstream observation point, the propagation distance d_D is then reduced and the radiation angle θ_D widens. In the same way, the radiation angle θ_S relative to the sideline point increases. The comparisons of the sound field properties of these three jets with those of the other jets, at points D and S, are therefore rather qualitative, and must be made with care.

The present variations in emission angles θ_D and θ_S are however expected to have small influence on the computed frequency peaks. For the downstream observation point, we can note for instance that in LESm09hre the Strouhal peaks at $\theta_D = 32.6°$ and at the angle $\theta = 38.6°$ for the point at $(x = 29r_0, r = 15r_0)$ were found [21] to be very close (0.29 versus 0.31). For the sideline point, we can likewise conjecture that, for a given jet, the spectral features of its sound field be quite similar over the range of emission angles θ_S. This is for instance supported by the spectra obtained for the LESm09re1700 jet at $\theta_S = 108.1°$ and at $\theta = 90°$ for the point at $(x = x_c, y = 15r_0, z = 0)$, presented in Figs. 12(a) and 13(b) respectively, which both show a peak for $\mathrm{St} = 0.19$. A similar behaviour is also probably observed for the azimuthal correlations for the present emission angles θ_S.

Finally, propagating acoustic waves may be dissipated by viscosity and thermal conductivity, depending on the Reynolds number and on the frequency involved. To evaluate the possible alterations of the sound field during propagation in the present study, the attenuation of plane sound waves is calculated for the different simulated jets following Pierce [31]. The distance of propagation considered is 20 radii, which is roughly the propagation distances d_B and d_S defined in Table 2. The values obtained are represented in Fig. 3a for the jets at Mach 0.9 and in Fig. 3b for the jets at Mach 0.6. For Strouhal numbers $0 \leq \mathrm{St} \leq 1.5$, the attenuation of sound waves is negligible for the two jets at $\mathrm{Re}_D \geq 10^5$, and is inferior to 1 dB for the low Reynolds number jets LESm09re10000, LESm09re5000, LESm06re3300 and LESm06re1700. For the jets LESm09re2500 and LESm09re1700, the attenuation appears higher than 1dB for about $\mathrm{St} \geq 1$ and $\mathrm{St} \geq 0.8$, respectively, but is still small for low Strouhal numbers.

The pressure spectra presented later in Figs. 7 and 12 being strongly dominated by low Strouhal number components, these dissipation plots indicate that the acoustic fields obtained at the points D and S are not appreciably affected during propagation. To illustrate this point more quantitatively, the attenuation of sound waves propagating over the distances d_D and d_S, at the peak frequencies observed at the points D and S, respectively, are provided in Table 3 for the different jets. It is found to be inferior to 0.1 dB in all the cases.

Table 3 Jets at Mach 0.9 (top) and at Mach 0.6 (bottom): attenuation of plane sound waves propagating over the distances d_D and d_S, calculated at the peak frequencies f_{peak} observed at the points D and S respectively

	$A(d_D, (f_{\text{peak}})_D)$	$A(d_S, (f_{\text{peak}})_S)$
LESm09hre	−0.01 dB	0
LESm09re10^4	−0.02 dB	−0.04 dB
LESm09re5000	−0.03 dB	−0.02 dB
LESm09re2500	−0.05 dB	−0.04 dB
LESm09re1700	−0.06 dB	−0.04 dB
LESm06hre	0	0
LESm06re3300	−0.01 dB	−0.01 dB
LESm06re1700	−0.02 dB	−0.01 dB

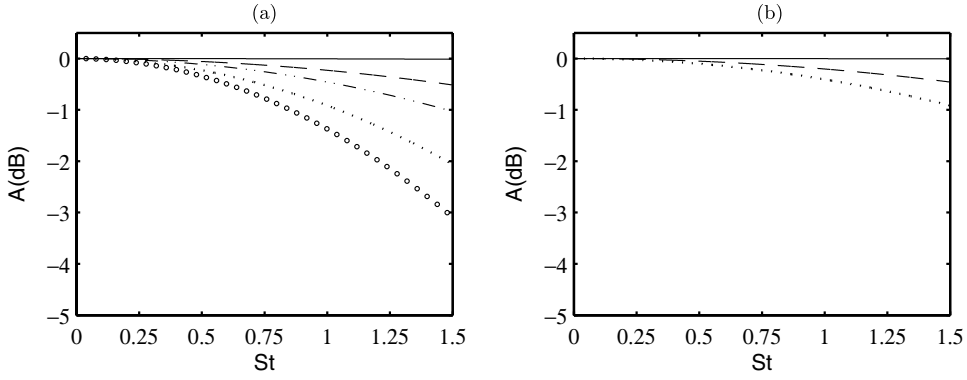

Fig. 3 Attenuation of plane sound waves propagating over 20 radii, as a function of Strouhal number St $= fD/u_j$, for: **a** Mach 0.9 jets, ——— LESm09hre, − − − LESm09re10^4, − · − · LESm09re5000, ····· LESm09re2500, ooooo LESm09re1700. **b** Mach 0.6 jets, ——— LESm06hre, − − − LESm06re3300, ····· LESm06re1700

3 Results

3.1 Instantaneous vorticity and pressure

Snapshots of the vorticity norm and of the fluctuating pressure are presented in Fig. 4 for the simulations LESm09hre, LESm09re5000, LESm09re2500 and LESm09re1700 at Mach 0.9 and in Fig. 5 for the simulations LESm06hre and LESm06re1700 at Mach 0.6. As the Reynolds number decreases, the jet flow changes significantly. At the high Reynolds numbers $\text{Re}_D \geq 10^5$ in LESm09hre and LESm06hre, the turbulent flow field shows a large range of vortical scales, whereas at lower Reynolds numbers, for instance at $\text{Re}_D = 1700$ in LESm09re1700 and LESm06re1700, a large part of the fine scales is lacking due to larger molecular dissipation scale. At low Reynolds numbers, viscosity also appears to affect appreciably the shear-layer development. In LESm09re1700 and LESm06re1700 for instance, the shear-layer thickness increases visibly by viscous diffusion. The generation of vortical structures in the shear layer occurs later, which must be related to the damping influence of viscosity on the growth rate of instability waves, reported notably by Michalke [32]. Another observation can be made at the very low Reynolds number of $\text{Re}_D = 1700$: the coherent turbulent structures appear in the shear layer close to the end of the potential core, with a length scale comparable to the jet radius, which may prevent vortex pairings. The effects of Mach and Reynolds numbers on the jet development are also illustrated by the core lengths x_c determined here from the centerline mean axial velocity u_c using $u_c(x_c) = 0.95u_j$, and given in Table 2 for the different jets. The length of the potential core is found to increase as the Reynolds number is lowered. At Mach 0.9 for instance, the core length is $10.2r_0$ for the jet at $\text{Re}_D \geq 10^5$, but $15.9r_0$ at $\text{Re}_D = 1700$. Moreover, the potential core shortens as the Mach number decreases, in agreement with experimental observations [33] and with the linear stability theory [32]. For the jets at $\text{Re}_D \geq 10^5$, the core length is thus $10.2r_0$ at Mach M $= 0.9$, but only $9.5r_0$ at M $= 0.6$. For completeness, note also that the Reynolds number is found to have the following influence on the jet development after the potential core: as the Reynolds number decreases, the jet development occurs more rapidly, with higher turbulence intensities, in good agreement with experimental data [34].

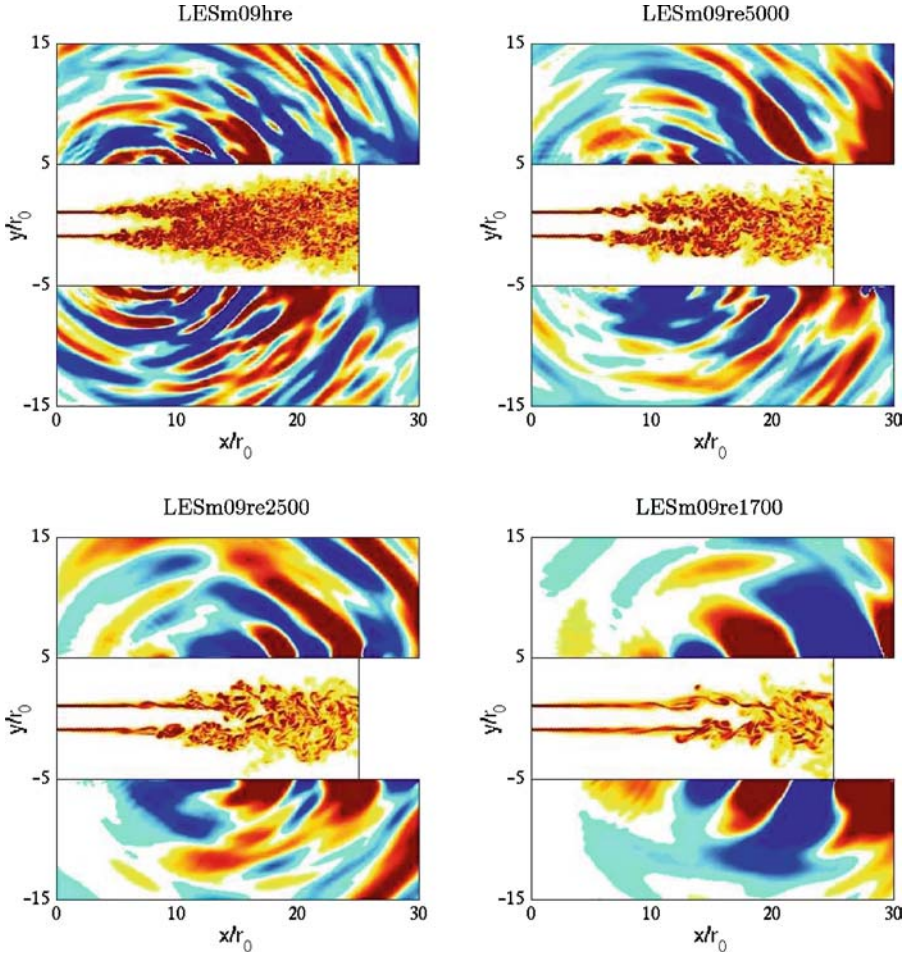

Fig. 4 Jets at Mach M = 0.9. Snapshots of the vorticity norm $|\boldsymbol{\omega}|$ in the flow and of the fluctuating pressure p' outside, in the plane $z = 0$, for LESm09hre, LESm09re5000, LESm09re2500 and LESm09re1700. For the four simulations, the color scale of the vorticity norm is $|\boldsymbol{\omega}| \times r_0/u_j = [0, 2.65]$, and the pressure color scale is $p' = [-70, 70]$ Pa or $p'/(\rho_j u_j^2) = [-6.2, 6.2] \times 10^{-4}$

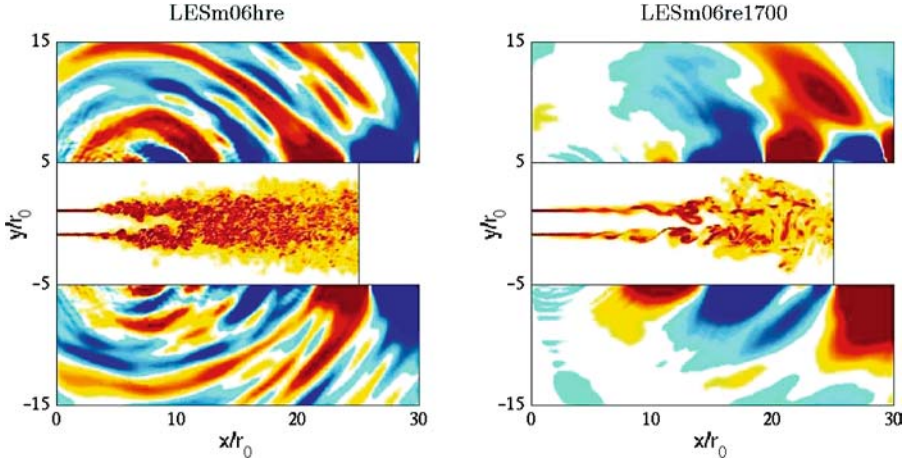

Fig. 5 Jets at Mach M = 0.6. Snapshots of vorticity and of pressure at $z = 0$ for LESm06hre and LESm06re1700. For both simulations, the color scale of the vorticity norm is $|\boldsymbol{\omega}| \times r_0/u_j = [0, 3]$, and the pressure color scale is $p' = [-20, 20]$ Pa or $p'/(\rho_j u_j^2) = [-4, 4] \times 10^{-4}$

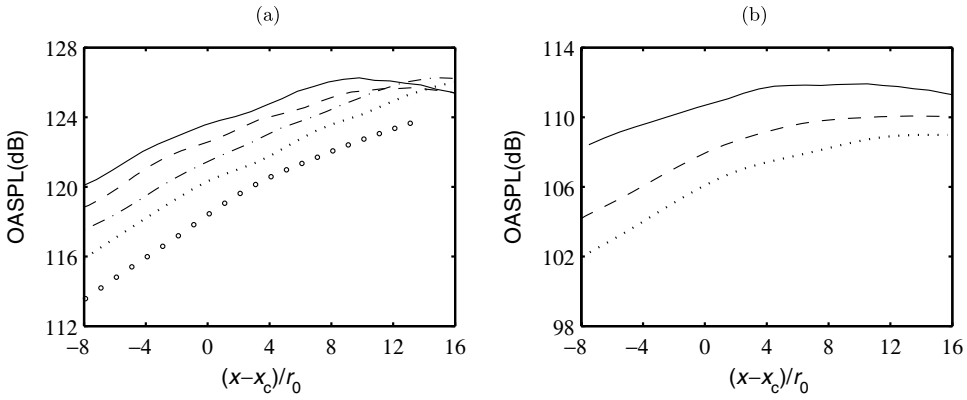

Fig. 6 Overall sound pressure levels along the line $r = 15r_0$, as a function of $x - x_c$, the axial position with respect to the end of the potential core. **a** Mach 0.9 jets, ——— LESm09hre, − − − LESm09re10^4, − · − · LESm09re5000, ····· LESm09re2500, ooooo LESm09re1700. **b** Mach 0.6 jets, ——— LESm06hre, − − − LESm06re3300, ····· LESm06re1700

The snapshots of Figs. 4 and 5 also display the important alterations of the radiated pressure field as the Mach and Reynolds numbers vary. First, as shown by the sound fields obtained for the two high Reynolds number jets LESm09hre and LESm06hre, the acoustic wavelengths are found to increase when the Mach number is lowered. Second, as for the turbulent field, the high-frequency sound waves appear to vanish progressively as the Reynolds number is decreased. Compare for instance the sound fields obtained at high Re_D in LESm09hre and at $\mathrm{Re}_D = 1700$ in LESm09re1700: short waves are clearly visible in the first case whereas only very low frequency waves remain in the second case. The disappearance of short waves at low Re_D visibly leads to a significant reduction of the sound levels for large radiation angles from the jet axis direction. We can moreover observe that spurious waves generated by the forcing are apparent near the inflow for the jets at Mach 0.6. Thanks to the forcing features [22], these waves have very short wavelengths, and they are damped by the explicit filtering. Their possible contributions to the acoustic field at $r = 15r_0$ are consequently very small.

The modifications of the noise magnitudes are shown quantitatively in Fig. 6 by the sound pressure levels along the line $r = 15r_0$ for the Mach 0.9 and Mach 0.6 jets. To take into account the different core lengths, these levels are represented as a function of the axial position with respect to the end of the potential core. The sound levels obtained for the various Reynolds numbers are similar around $x \simeq x_c + 15r_0$, for emission angles from the jet axis, relative to an origin at the end of the jet core, of $\theta \simeq 45^\circ$. However they are quite scattered at $x \leq x_c + 10r_0$, for larger angles. A difference of 4 dB is for instance noticed between the levels obtained at $x = x_c$ for the Mach 0.9 jets at high Re_D and at $\mathrm{Re}_D = 2500$. These changes are in good agreement with the experimental data [16] provided for two Mach 0.9 jets at $\mathrm{Re}_D = 3600$ and $\mathrm{Re}_D = 5.4 \times 10^5$, displaying very little difference between far-field sound levels at 30° from the nozzle exit, but 4 dB at 90°.

3.2 Downstream sound field

The properties of the downstream pressure fields radiated by the jets are investigated at the observation point D located at $x_D = 29r_0, r_D = 12r_0$.

3.2.1 Downstream sound spectra

The sound spectra calculated at the point D for the Mach 0.9 and Mach 0.6 jets are presented in Fig. 7a and 7b, in linear scales, as a function of the Strouhal number. Their shapes appear to change moderately with the Reynolds number. All spectra are indeed dominated by a low-frequency component at Strouhal number $\mathrm{St} \simeq 0.25$. The peak seems however more marked with respect to the high-frequency components of the spectra at low Reynolds numbers. This trend is clearly illustrated in Fig. 7a by the spectra obtained for the Mach 0.9 jets at high-Re_D (solid line) and at $\mathrm{Re}_D = 2500$ (dotted line). As for the peak amplitude, for both Mach numbers, it is found to increase as the Reynolds number decreases, as shown for instance by the spectra

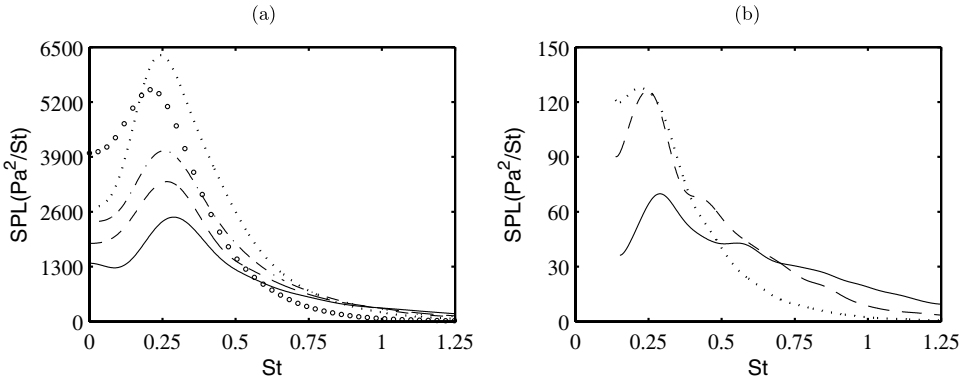

Fig. 7 Downstream pressure spectra at $x_D = 29r_0$ and $r_D = 12r_0$, as a function of Strouhal number $\mathrm{St} = fD/u_j$. **a** Mach 0.9 jets, ——— LESm09hre, − − − LESm09re10^4, − · − · LESm09re5000, ····· LESm09re2500, ooooo LESm09re1700. **b** Mach 0.6 jets, ——— LESm06hre, − − − LESm06re3300, ····· LESm06re1700

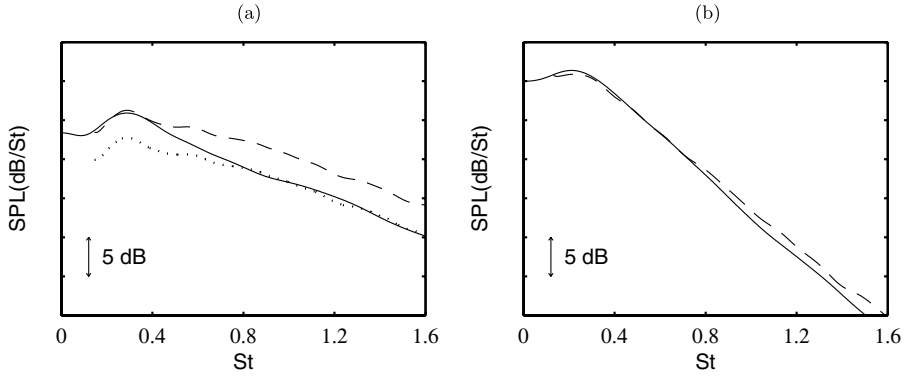

Fig. 8 Downstream pressure spectra at $x_D = 29r_0$ and $r_D = 12r_0$. **a** Jets at $\mathrm{Re}_D > 10^5$: ——— LESm09hre; − − − LESm06hre, using a $(0.9/0.6)^9$ scaling factor for the levels; ····· LESm06hre, using a $(0.9/0.6)^7$ scaling factor. **b** Jets at $\mathrm{Re}_D = 1700$: ——— LESm09re1700; − − − LESm06re1700, using a $(0.9/0.6)^9$ scaling factor

of the Mach 0.9 jets LESm09hre, LESm09re10000 and LESm09re5000 for which the core length is nearly constant.

To evaluate the variations of sound spectra with velocity, the spectra obtained at similar Reynolds numbers are depicted in Fig. 8, in logarithmic scales, using different scaling factors to correct the sound levels of the Mach 0.6 jets. At high Reynolds numbers $\mathrm{Re}_D > 10^5$, in Fig. 8a, the peak levels are shown to vary as u_j^9, whereas the high-frequency parts of the spectra for $\mathrm{St} \geq 0.8$ collapse successfully following a u_j^7 scaling. These results agree well with the experimental far-field observations at high Reynolds numbers. Zaman and Yu [11] and Tam et al. [2] both noticed for instance a $u_j^{9.5}$ variation of the peak level, at 30° and 20° to the jet axis respectively. In the spectra reported by Zaman and Yu [11], the levels of the high-frequency components were also seen to increase at a lower exponent, as observed in Mollo-Christensen et al. [1] This difference of variations between low and high frequency levels however does not seem to exist for the spectra at $\mathrm{Re}_D = 1700$ in Fig. 8b. In this case, the power law of u_j^9 applies fairly well not only for the peak but also for the whole frequency range. Finally we can note the different decrease of the sound levels towards high Strouhal numbers as the Reynolds number is reduced: at Mach 0.9 for instance, the gap between the peak and the $\mathrm{St} = 1.5$ levels is 15 dB at high Re_D, but 30 dB at $\mathrm{Re}_D = 1700$.

The peak frequencies are now represented as a function of the Reynolds number. In Fig. 9a, they are shown to collapse well using Strouhal number scaling. The peak Strouhal number is found to decrease slightly at lower Reynolds numbers, with for instance $\mathrm{St}_{\mathrm{peak}} = 0.29$ at high Re_D versus $\mathrm{St}_{\mathrm{peak}} = 0.22$ at $\mathrm{Re}_D = 1700$. In Fig. 9b, Helmholtz number scaling is also displayed, and it is clearly seen to be inappropriate.

For completeness, the scaling with the Helmholtz number times the Doppler factor $(1 - \mathrm{Mc}\cos\theta)$, where Mc is assumed to be the source convection Mach number, is tested in Fig. 10. Zaman and Yu [11] observed

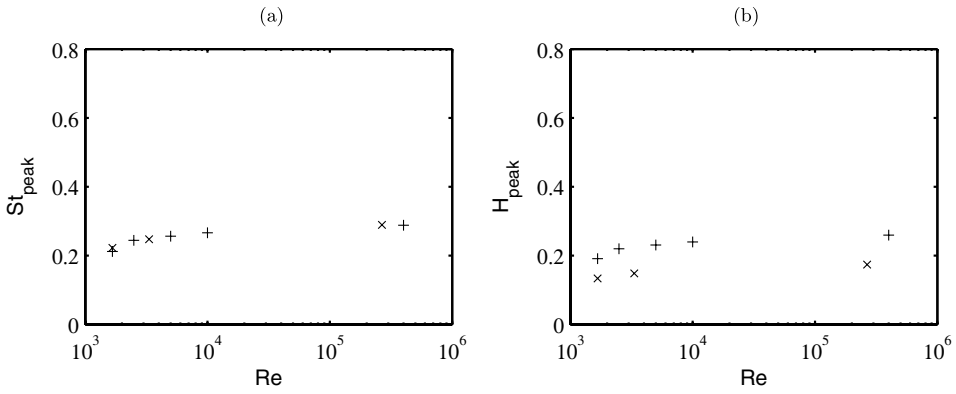

Fig. 9 Scaling with Reynolds number of the pressure spectrum peaks obtained at $x_D = 29r_0$ and $r_D = 12r_0$ for jets at: + Mach 0.9; × Mach 0.6. **a** Peak Strouhal numbers $\mathrm{St}_{\mathrm{peak}} = f_{\mathrm{peak}} D/u_j$. **b** Peak Helmholtz numbers $\mathrm{H}_{\mathrm{peak}} = f_{\mathrm{peak}} D/c_0$

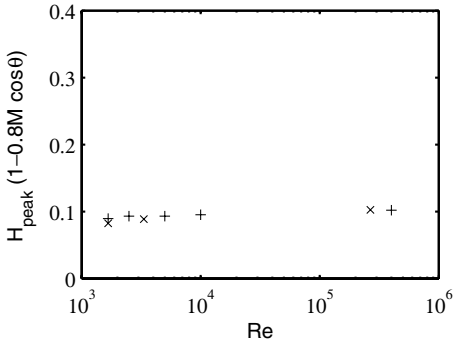

Fig. 10 Scaling with Reynolds number of the pressure spectrum peaks $\mathrm{H}_{\mathrm{peak}}(1 - 0.8\mathrm{M}\cos\theta)$ obtained at $x_D = 29r_0$ and $r_D = 12r_0$. See caption of Fig. 9 for the symbols

that the best collapse of the spectra for shallow angles is yielded for Mc = 0.5 M. In the present work, with $\theta = \theta_D$ calculated from the end of the potential core and given in Table 2, the best scaling is obtained for Mc = 0.8 M. This scaling is shown in Fig. 10. It is therefore difficult to settle the matter of Strouhal scaling versus Helmholtz times a Doppler factor scaling for the downstream sound spectra. However the latter scaling depends on the choice of the parameter Mc, and still needs physical justifications if it is not to appear only as an *ad hoc* scaling.

3.2.2 Downstream azimuthal correlations

To study the structure of the downstream sound field, the azimuthal cross-correlation functions of the fluctuating pressure are calculated at the observation point D. The functions obtained for the Mach 0.9 jets LESm09hre, LESm09re10000 and LESm09re5000, for which the emission angles θ_D are very close as shown in Table 2, are presented in Fig. 11a. They display high correlation levels in good agreement with the far-field correlation functions measured by Maestrello [35] at 30° to the jet axis for a Mach 0.85 jet. Moreover they do not differ appreciably, which suggests that the influence of the Reynolds number on the azimutal cross-correlations in the downstream direction is small.

The correlation functions obtained for the two high Reynolds number jets at Mach 0.6 and 0.9 are presented in Fig. 11(b). The correlation obtained at Mach 0.6 is slightly higher for $\phi \leq 90°$ but lower for $\phi \geq 90°$ compared to that obtained at Mach 0.9. This trend corresponds well to far-field measurements [35, 36] at 30° to the jet axis.

Finally the modal contribution to the downstream sound field is provided in Table 4 for the two high Re_D jets. In both jets, the modes $m = 0$ and $m = 1$ are greatly dominant with more than 90% of the total acoustic field, including 66% for the mode $m = 0$ alone. The influence of the Mach number on the azimuthal Fourier components is also shown with, mainly, a decrease of the contribution of the mode $m = 1$ as the Mach number

Table 4 Contributions to the acoustic field at $x_D = 29r_0$ and $r_D = 12r_0$ of the first four azimuthal modes for the jets at $\mathrm{Re}_D > 10^5$

	$m = 0$	$m = 1$	$m = 2$	$m = 3$
LESm09hre	0.67	0.23	0.07	0.02
LESm06hre	0.66	0.28	0.05	0.01

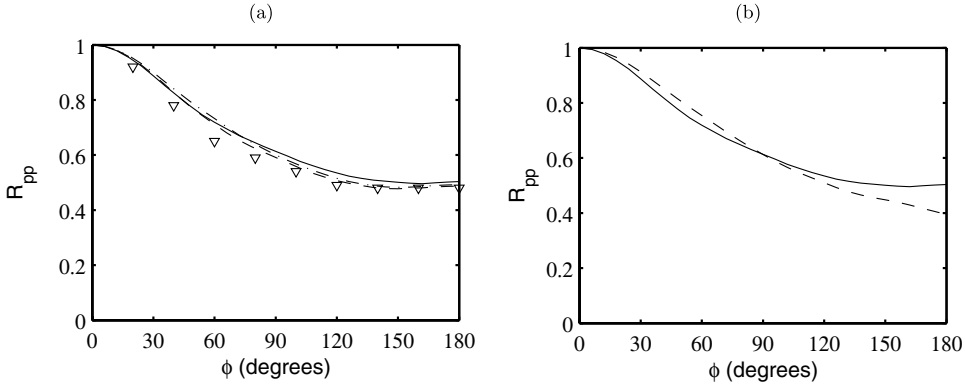

Fig. 11 Azimuthal cross-correlations of the fluctuating pressure at $x_D = 29r_0$ and $r_D = 12r_0$. **a** For the Mach 0.9 jets: ——— LESm09hre, − − − LESm09re10^4, − · − · LESm09re5000. **b** For the jets at $\mathrm{Re}_D > 10^5$: ——— LESm09hre, − − − LESm06hre. Far-field measurements at 30° from the jet axis: ▽ Maestrello [35] ($\mathrm{M} = 0.85$, $\mathrm{Re}_D = 5 \times 10^5$)

increases. These results are very similar to the far-field experimental data obtained by Juvé and Sunyach [36] at 30° to the jet axis.

3.3 Sideline sound field

The sound fields obtained in the sideline direction are now studied, in particular at the observation point S located at $x_S = 11r_0, r_S = 15r_0$.

3.3.1 Sideline sound spectra

The sound spectra calculated at point S are presented in Fig. 12a and b for the Mach 0.9 and the Mach 0.6 jets, in linear scales, as a function of the Strouhal number. As the Reynolds number decreases, they change spectacularly with the disappearance of the high-frequency components. Moreover the lower the Reynolds number, the larger the part of the spectra that vanishes. Consequently, the peak frequency progressively moves to lower Strouhal numbers, with for instance for the Mach 0.9 jets $\mathrm{St}_{\mathrm{peak}} = 0.7$ at $\mathrm{Re}_D = 4 \times 10^5$ but only $\mathrm{St}_{\mathrm{peak}} = 0.2$ at $\mathrm{Re}_D = 1700$. For these two jets, we can note also the significant reduction in spectral bandwidths: about $0 \leq \mathrm{St} \leq 1.5$ versus $0 \leq \mathrm{St} \leq 0.4$.

The variations of the sound spectra with velocity are shown in Fig. 13 where the spectra obtained at similar Reynolds numbers are depicted, in logarithmic scales, using the appropriate scaling factor to correct the sound levels of the Mach 0.6 jets. The spectra of the high Reynolds number jets at Mach numbers 0.6 and 0.9 at the observation point S are presented in Fig. 13a. They collapse very well over the whole frequency range following a $u_j^{7.5}$ scaling. This $u_j^{7.5}$ power law is exactly that exhibited experimentally by Zaman & Yu [11] and Tam *et al.* [2] for far-field spectra at 90° to the jet axis, for high Reynolds number jets. To examine the levels of the sideline noise radiated by the jets at $\mathrm{Re}_D = 1700$, the pressure spectra obtained at $y = 15r_0$, $z = 0$, at the axial location of the end of the potential core $x = x_c$, are considered. They are plotted in Fig. 13b. As previously noted at high Reynolds numbers, the two spectra at Mach 0.6 and 0.9 collapse well using a $u_j^{7.5}$ scaling factor to adjust the levels of the Mach 0.6 jet. The agreement is found to be particularly good for the frequency peaks.

The Strouhal number and Helmholtz number peaks obtained at the sideline point S are now represented in Fig. 14 as a function of the Reynolds number. The Strouhal number scaling appears to apply at high Reynolds

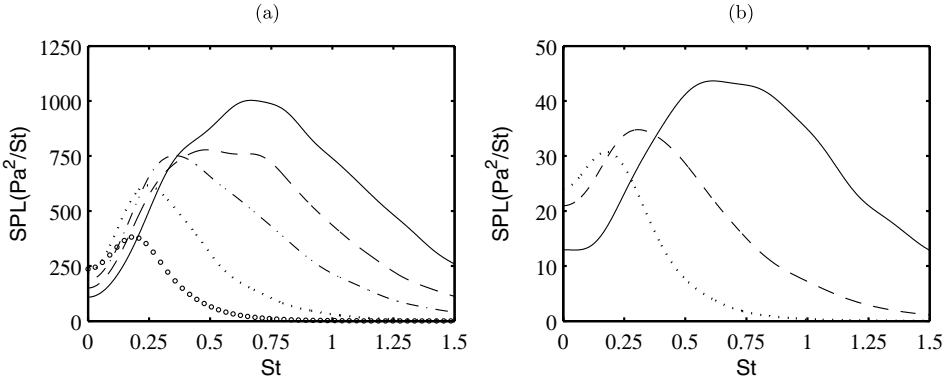

Fig. 12 Sideline pressure spectra at $x_S = 11r_0$ and $r_S = 15r_0$, as a function of Strouhal number $\mathrm{St} = fD/u_j$. **a** Mach 0.9 jets, ——— LESm09hre, − − − LESm09re10^4, − · − · LESm09re5000, ····· LESm09re2500, ooooo LESm09re1700. **b** Mach 0.6 jets, ——— LESm06hre, − − − LESm06re3300, ····· LESm06re1700

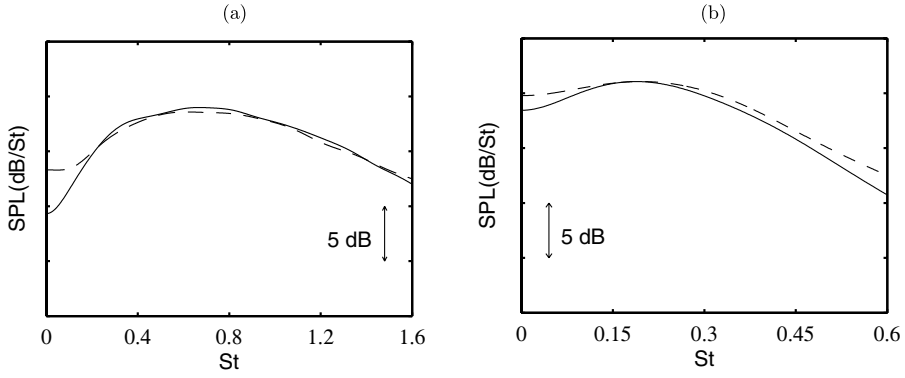

Fig. 13 Sideline pressure spectra. **a** For the jets at $\mathrm{Re}_D > 10^5$, at $x_S = 11r_0$ and $r_S = 15r_0$: ——— LESm09hre; − − − LESm06hre, using a $(0.9/0.6)^{7.5}$ scaling factor for the levels. **b** For the jets at $\mathrm{Re}_D = 1700$, at $x = x_c$, $y = 15r_0$ and $z = 0$: ——— LESm09re1700; − − − LESm06re1700, using a $(0.9/0.6)^{7.5}$ scaling factor

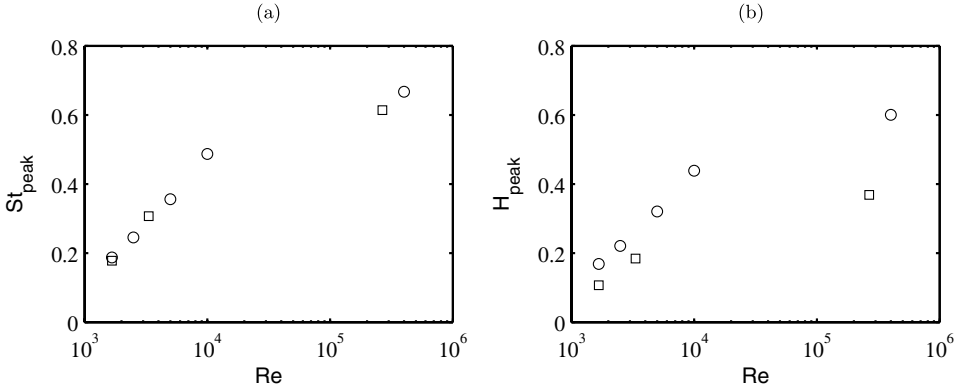

Fig. 14 Scaling with Reynolds number of the pressure spectrum peaks obtained at $x_S = 11r_0$ and $r_S = 15r_0$ for jets at: o Mach 0.9; □ Mach 0.6. **a** Peak Strouhal numbers $\mathrm{St}_{\mathrm{peak}} = f_{\mathrm{peak}} D/u_j$. **b** Peak Helmholtz numbers $\mathrm{H}_{\mathrm{peak}} = f_{\mathrm{peak}} D/c_0$

Table 5 Contributions to the acoustic field at $x_S = 11r_0$ and $r_S = 15r_0$ of the first five azimuthal modes for the jets at $\mathrm{Re}_D > 10^5$ (top) and $\mathrm{Re}_D = 1700$ (bottom)

	$m=0$	$m=1$	$m=2$	$m=3$	$m=4$
LESm09hre	0.15	0.29	0.23	0.19	0.09
LESm06hre	0.15	0.35	0.28	0.17	0.05
LESm09re1700	0.34	0.36	0.23	0.05	0.03
LESm06re1700	0.40	0.23	0.32	0.05	–

numbers, as found experimentally by Mollo-Christensen *et al.* [1], but also at low Reynolds numbers as clearly shown by the frequency peaks obtained for the two jets at $\mathrm{Re}_D = 1700$. As a result, the Helmholtz scaling is not appropriate. This point seems to contradict the experimental data of Long and Arndt [17] at low Reynolds numbers, which display an Helmholtz scaling at the radiation angle of 90° in the far acoustic field. As for the variation of the frequency peak with the Reynolds number, the peak progressively moves to lower Strouhal numbers as the Reynolds number decreases. Note that at sufficiently high Reynolds numbers, typically $\mathrm{Re}_D \geq 10^5$, the Strouhal peak is expected to be nearly constant. Zaman and Yu [11] indeed observed that, for jets with Reynolds numbers over the range $2 \times 10^5 \leq \mathrm{Re}_D \leq 2.1 \times 10^6$, the Strouhal number peaks measured in the far acoustic field at 90° to the jet axis do not vary significantly.

3.3.2 Sideline azimuthal correlations

The azimuthal cross-correlation functions of the sound field at the sideline observation point are presented in Fig. 15 for the high Reynolds number jets and for the $\mathrm{Re}_D = 1700$ jets. At high Reynolds numbers in Fig. 15a, the correlation functions at Mach 0.6 and Mach 0.9 do not differ much. They show low correlation levels, in agreement with experimental data for sideline radiation angles, notably with those measured by Maestrello [35, 36] for a Mach 0.7 jet. At $\mathrm{Re}_D = 1700$, in Fig. 15b, the correlation levels are found to be higher, especially for large azimuthal angles as illustrated by the correlations obtained at $\phi = 180°$ for the Mach 0.6 jets (nearly 0 at high Reynolds number versus 0.4 at $\mathrm{Re}_D = 1.7 \times 10^3$). The correlation then appears to be enhanced as the Reynolds number decreases, Furthermore, at $\mathrm{Re}_D = 1700$, the correlations obtained at Mach 0.6 and 0.9 are close except for angles $\phi \simeq 180°$ where the correlation is higher at the lower Mach number. A similar trend was found experimentally by Juvé and Sunyach [36] for the sideline noise radiated by jets at Mach numbers 0.4 and 0.7.

Finally, the modal contribution to the sideline acoustic field is reported in Table 5 for the jets at $\mathrm{Re}_D \geq 10^5$ and at $\mathrm{Re}_D = 1700$. The azimuthal Fourier components are shown to depend significantly on the Reynolds number. At $\mathrm{Re}_D \geq 10^5$, the modes $m = 1$ and $m = 2$ are dominant, in agreement with the far-field measurements of Juvé & Sunyach [36] at 90° to the jet axis for a high Reynolds number jet at Mach 0.7. The mode $m = 0$ then contains only 15% of the total sound field, and the mode $m = 3$ about 18%. At $\mathrm{Re}_D = 1700$, the

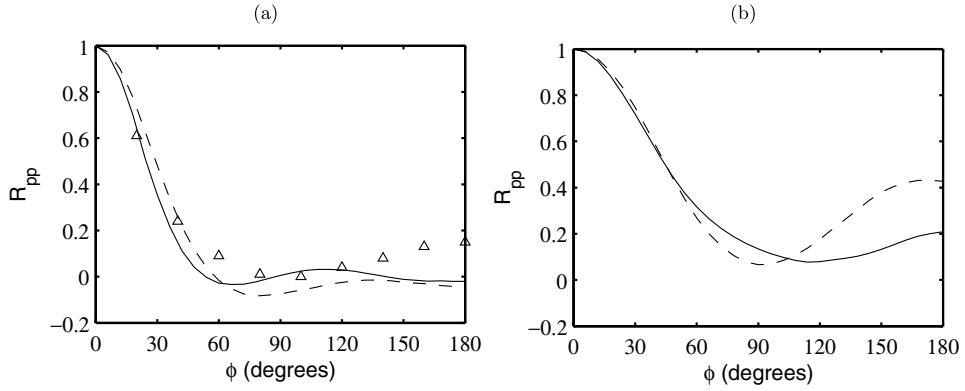

Fig. 15 Azimuthal cross-correlations of the fluctuating pressure obtained at $x_S = 11r_0$ and $r_S = 15r_0$ for: **a** The jets at $\mathrm{Re}_D > 10^5$. **b** The jets at $\mathrm{Re}_D = 1700$; at: ——— Mach 0.9, – – – Mach 0.6. Far-field measurements at 90° from the jet axis: △ Maestrello [35, 36] ($\mathrm{M} = 0.7$, $\mathrm{Re}_D = 4.3 \times 10^5$)

contribution of the mode $m = 0$ is however greatly enhanced and is more than 30%, while that of the mode $m = 3$ falls down to 5%. As for the Mach number, its main effect on the modal contribution to the sideline sound field is found to be the decrease of the mode $m = 2$ as the Mach number increases, which corresponds well to experimental data [36].

4 Discussion on sound sources

The modifications of the sound field obtained in the present simulations in the downstream and sideline directions as the Mach and Reynolds numbers vary bring support to the theory of two sound sources in subsonic jets. They also provide information about features of the radiations generated by these two basic noise mechanisms.

There first appears to be a Reynolds number-dependent sound source dominating in the sideline direction. The noise radiated by this source is broadband and poorly azimuthally correlated. Above all, this radiation depends strongly on the Reynolds number. At lower Reynolds numbers, its amplitude decreases dramatically, the sound spectra become narrower with a frequency peak moving to lower Strouhal numbers, and the azimuthal correlations are slightly enhanced. This radiation seems to be predominant in the sideline direction for the whole frequency range at high Reynolds numbers, in agreement with experimental data, but also at the low Reynolds numbers considered in this study. This point is supported by the sideline spectra reported in Fig. 13 for Mach 0.6 and Mach 0.9 jets at Reynolds numbers $\mathrm{Re}_D \geq 10^5$ and $\mathrm{Re}_D = 1700$. For both Reynolds numbers, these spectra are indeed found to scale in frequency with the Strouhal number. The Helmholtz scaling suggested by certain experimental data at low Reynolds number [17] is in particular not appropriate at $\mathrm{Re}_D = 1700$. Furthermore, the sideline sound levels vary with velocity as $u_j^{7.5}$ at $\mathrm{Re}_D \geq 10^5$, following the power law exhibited experimentally for high Reynolds number jets at 90° to the jet axis [2, 11], but also at $\mathrm{Re}_D = 1700$. It is also interesting to note that this radiation appears to contribute appreciably to the high frequency part of the downstream spectra, at high Reynolds numbers at least, as shown in Fig. 8. This radiation is thus observed both in the sideline and the downstream directions, which suggests that its directivity is not highly marked.

To identify the source responsible for this broadband, Reynolds number-dependent radiation, it is tempting to infer from the present results that this radiation tends to vanish at very low Reynolds number, as vortical structures disappear. The sound source involved is therefore naturally the turbulence developing randomly in the jet. The randomly-developing turbulence refers to all the vortical structures interacting randomly with one another, whose sizes range from the larger scale given by the flow geometry, here the jet diameter, down to the smallest one, namely the Kolmogorov scale, which increases as the Reynolds number decreases. It corresponds to the so-called fine-scale turbulence in the works of Tam *et al.* [2, 37] and Viswanathan [7], whose associated noise was shown to dominate at 90° to the jet axis, and to depend on the jet Reynolds number. It can be also noted that the noise radiated by this source is certainly that obtained using the approaches based on Lighthill's or Lilley's acoustic analogies and/or modellings of the statistical properties of the turbulent sources [37, 38, 39], which predict the sideline acoustic spectra successfully.

The sound sources associated with the randomly-developing turbulence cannot be easily localized since they are expected to be distributed all along the jet, and their locations may depend on the frequency considered. However, as suggested by near-field pressure measurements [28], the high-frequency sources, typically with $\mathrm{St} \geq 0.5$, may be particularly active in the jet shear layer. This view is supported by the snapshots of Figs. 4 and 5 at high Reynolds numbers, showing that a significant part of the high frequency noise is generated upstream of the end of the potential core. It is also supported by recent high Reynolds number simulations where a correlation between the peaks of turbulence intensities in the shear layer and the sound levels in the sideline direction was found [22]. As for the generation mechanisms themselves, the rapid evolution of vortices whithin the mixing layer during specific events such as pairing or tearing [20, 40] can be mentioned.

A second, deterministic sound source is clearly observed in the downstream direction. Unlike the first source, the radiation generated by this source is not very sensitive to the Reynolds number. For all Reynolds numbers indeed, the spectra at the downstream observation point are dominated by well-marked peaks at the low Strouhal number $\mathrm{St} \simeq 0.25$, with levels rather similar, and the azimuthal cross-correlations are high. Another difference with the noise radiated by the randomly-developing turbulence is the scaling with velocity of the peak levels, which follows a power law at a higher exponent. This radiation appears also highly directional. There is indeed no indication that it contributes to the sideline noise radiated by the present simulated jets, even at the lower Reynolds numbers. The latter point is supported by the scaling of sideline sound levels

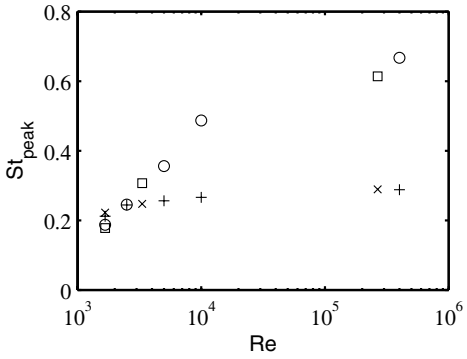

Fig. 16 Scaling with Reynolds number of the peak Strouhal numbers obtained in the downstream direction for the + Mach 0.9 and × Mach 0.6 jets, and in the sideline direction for the o Mach 0.9 and □ Mach 0.6 jets

with velocity, presented in Fig. 13, which is exactly the same at $\mathrm{Re}_D \geq 10^5$ and at $\mathrm{Re}_D = 1700$. It is also illustrated in Fig. 16 where the Strouhal number peaks obtained in the downstream and sideline directions are plotted as a function of the Reynolds number. As the Reynolds number decreases, the Strouhal peak in the sideline direction becomes smaller, down to $\mathrm{St} = 0.19$ at $\mathrm{Re}_D = 1700$, but it does not degenerate in a convincing manner to the Strouhal number observed downstream for the deterministic radiation, which is for instance $\mathrm{St} = 0.22$ at $\mathrm{Re}_D = 1700$.

The present simulation results show that the deterministic jet noise source is nearly independent of the jet turbulence. This source must therefore be connected to a mechanism intrinsic to the jet geometry, and must only involve the larger structures of the jet, typically of the size of the jet radius. These larger structures are often referred to as coherent structures, and they are usually related to the instability waves growing/decaying in the shear layer. In the jet noise theory of Tam *et al*. [2] for instance, the downstream, highly directional noise component observed from experimental data, corresponding to the present deterministic radiation, is thus attributed to large turbulence structures/instability waves. However the basic mechanism of this sound source is still subject to discussion. The generation of noise by the rapid growth and decay of instability waves in the jet was for instance proposed and investigated analytically [8, 9]. It is interesting to notice that this mechanism is likely to generate a highly directional radiation. The intrusion of vortical structures in the potential core, occurring periodically at a frequency corresponding to the frequency of the deterministic noise, was also suggested by the authors [20] from simultaneous sound-flow visualizations issued from simulations. Moreover, if the deterministic jet noise mechanism is still to be definitively identified and comprehensively described, its location appears well established. Experimental sound source localizations [41] shown for instance that most of the downstream noise is generated just downstream of the potential core. Significant direct correlations have also been found between the downstream pressure and the flow fluctuations on the jet axis at the end of the potential core, experimentally by Schaffar [42] and Panda *et al*. [43, 44] and from the present simulation results [45].

5 Conclusion

In the present paper, the sound fields generated by subsonic jets at different Mach and Reynolds numbers have been calculated directly by Large Eddy Simulation, and compared in order to investigate the properties of jet noise sources. The following conclusions are reached.

Two distinct radiation patterns are observed. The first radiation dominates for large angles from the jet direction. It is broadband and poorly azimuthally correlated. The second radiation dominates for shallow angles and is negligible for large angles. It appears as a low-frequency peak at a fixed Strouhal number, and is highly azimuthally correlated.

As the Reynolds number decreases, for the radiation predominant in the sideline direction, the sound levels diminish significantly, a large high-frequency part of the sound spectra disappears, and the levels of azimuthal correlation are slightly enhanced, whereas the properties of the downstream radiation do not change appreciably.

As the jet velocity varies, spectra of both radiations are seen to scale in frequency with the Strouhal number. However the scalings of levels differ: the levels of the Reynolds number-dependent radiation follow a power law of $u_j^{7.5}$ whereas those of the downstream radiation follow a power law at a higher exponent.

These observations strongly support the presence of two basic components in subsonic jet noise: a Reynolds number-dependent source, responsible for the sideline radiation, connected to the randomly-developing turbulence, and a deterministic source, radiating only in the downstream direction, associated to a mechanism intrinsic to the jet geometry at the end of the potential core, which is still to be clearly described.

Acknowledgements This work was supported by the French network RRIT "Recherche Aéronautique sur le Supersonique" (Ministère de la Recherche). Computing time is supplied by the Institut du Développement et des Ressources en Informatique Scientifique (IDRIS - CNRS). We are grateful to one of the referees for particularly helpful comments.

References

1. Mollo-Christensen, E., Kolpin, M.A., Martucelli, J.R.: Experiments on jet flows and jet noise far-field spectra and directivity patterns. J. Fluid Mech. **18**, 285–301 (1964)
2. Tam, C.K.W., Golebiowski, M., Seiner, J.M.: On the two components of turbulent mixing noise from supersonic jets. AIAA Paper 96-1716 (1996)
3. Tam, C.K.W.: Supersonic jet noise. Annu. Rev. Fluid Mech. **27**, 17–43 (1995)
4. Tam, C.K.W.: Jet noise: since 1952. Theoret. Comput. Fluid Dynamics **10**, 393–405 (1998)
5. Lilley, G.M.: Jet noise classical theory and experiments. In: Aeroacoustics of Flight Vehicles, H.H. Hubbard (ed.), Vol. 1: Noise Sources, 211–289 (1994)
6. Viswanathan, K.: Analysis of the two similarity components of turbulent mixing noise. AIAA Journal **40**(9), 1735–1744 (2002)
7. Viswanathan, K.: Aeroacoustics of hot jets. J. Fluid Mech. **516**, 39–82 (2004)
8. Cooper, A.J., Crighton, D.G.: Global modes and superdirective acoustic radiation in low-speed axisymmetric jets, Eur. J. Mech. B-Fluids **19**, 559–574 (2000)
9. Goldstein, M.E., Leib, S.J.: The role of instability waves in predicting jet noise. J. Fluid Mech. **525**, 37–72 (2005)
10. Viswanathan, K.: Jet aeroacoustic testing: issues and implications. AIAA Journal **41**(9), 1674–1689 (2003)
11. Zaman, K.B.M.Q., Yu, J.C.: Power spectral density of subsonic jet noise. J. Sound Vib. **98**(4), 519–537 (1985)
12. Crighton, D.G.: Acoustics as a branch of fluid mechanics. J. Fluid Mech. **106**, 261–298 (1981)
13. Lush, P.A.: Measurements of subsonic jet noise and comparison with theory. J. Fluid Mech. **46**(3), 477–500 (1971)
14. Ahuja, K.K.: Correlation and prediction of jet noise. J. Sound Vib. **29**(2), 155–168 (1973)
15. Tanna, H.K.: An experimental study of jet noise. Part I: Turbulent mixing noise. J. Sound Vib. **50**(3), 405–428 (1977)
16. Stromberg, J.L., McLaughlin, D.K., Troutt, T.R.: Flow field and acoustic properties of a Mach number 0.9 jet at a low Reynolds number. J. Sound. Vib. **72**(2), 159–176 (1980)
17. Long, D.F., Arndt, R.E.A: Jet noise at low Reynolds number. AIAA Journal **22**(2), 187–193 (1984)
18. Morrison G.L., McLaughlin, D.K.: Noise generation by instabilities in low Reynolds number supersonic jets. J. Sound Vib. **65**(2), 177–191 (1979)
19. Freund, J.B.: Noise sources in a low-Reynolds-number turbulent jet at Mach 0.9. J. Fluid Mech. **438**, 277–305 (2001)
20. Bogey, C., Bailly, C., Juvé, D.: Noise investigation of a high subsonic, moderate Reynolds number jet using a compressible LES. Theoret. Comput. Fluid Dynamics **16**(4), 273–297 (2003)
21. Bogey, C., Bailly, C.: Computation of a high Reynolds number jet and its radiated noise using LES based on explicit filtering. Computers and Fluids (2006)
22. Bogey, C., Bailly, C.: Effects of inflow conditions and forcing on subsonic jet flows and noise. AIAA Journal **43**(5), 1000–1007 (2005)
23. Bogey, C., Bailly, C.: Decrease of the effective Reynolds number with eddy-viscosity subgrid-scale modeling. AIAA Journal **43**(2), 437–439 (2005)
24. Bogey, C., Bailly, C.: A family of low dispersive and low dissipative explicit schemes for flow and noise computations. J. Comput. Phys. **194**(1), 194–214 (2004)
25. Rizzetta, D.P., Visbal, M.R., Blaisdell, G.A.: A time-implicit high-order compact differencing and filtering scheme for large-eddy simulation. Int. J. Num. Meth. Fluids **42**(6), 665–693 (2003)
26. Bogey, C., Bailly, C.: Three-dimensional non reflective boundary conditions for acoustic simulations: far-field formulation and validation test cases. Acta Acustica **88**(4), 463–471 (2002)
27. Zaman, K.B.M.Q.: Far-field noise of a subsonic jet under controlled excitation. J. Fluid Mech. **152**, 83–111 (1985)
28. Zaman, K.B.M.Q.: Flow field and near and far sound field of a subsonic jet. J. Sound Vib. **106**(1), 1–16 (1986)
29. Ukeiley, L.S., Ponton, M.K.: On the near field pressure of a transonic axisymmetric jet. Int. J. of Aeroacoustics **3**(1), 43–66 (2004)
30. Arndt, R.E.A, Long, D.F., Glauser, M.N.: The proper orthogonal decomposition of pressure fluctuations surrounding a turbulent jet. J. Fluid Mech. **340**, 1–33 (1997)
31. Pierce A.D: Acoustics-An introduction to its physical principles and applications. Acoustical society of America, Woodbury, NY, 517–519 (1989)
32. Michalke, A.: Survey on jet instability theory. Prog. Aerospace Sci. **21**, 159–199 (1984)
33. Lau, J.C.: Effects of exit Mach number and temperature on mean-flow and turbulence characteristics in round jets. J. Fluid Mech. **105**, 193–218 (1981)

34. Bogey, C., Bailly, C.: Large Eddy Simulations of round free jets using explicit filtering with/without dynamic Smagorinsky model. Fourth International Symposium on Turbulence and Shear Flow Phenomena **2**, 817–822 (2005). To appear in Int. J. Heat Fluid Flow (2006).
35. Maestrello, L.: Two points correlations of sound pressure in the far field of a jet: Experiment. NASA-TMX-72835 (1976)
36. Juvé, D., Sunyach, M.: Structure azimutale du champ acoustique lointain d'un jet subsonique. C. R. Acad. Sc. Paris, t. 287, série B, 187–90 (1978) (in french)
37. Tam, C.K.W., Auriault, L.: Jet mixing noise from fine-scale turbulence. AIAA Journal **37**(2), 145–155 (1999)
38. Morris, P.J., Farassat, F.: Acoustic analogy and alternative theories for jet noise prediction. AIAA Journal **40**(4), 671–680 (2002)
39. Golsdtein, M.E.: Ninety-degree acoustic spectrum of a high-speed air jet. AIAA Journal **43**(1), 96–102 (2005)
40. Hileman, J., Samimy, M.: Turbulence structures and the acoustic far field of a Mach 1.3 jet. AIAA Journal **39**(9), 1716–1727 (2001)
41. Juvé, D., Sunyach, M., Comte-Bellot, G.: Intermittency of the noise emission in subsonic cold jets. J. Sound Vib. **71**, 319–32 (1980)
42. Schaffar, M.: Direct measurements of the correlation between axial in-jet velocity fluctuations and far field noise near the axis of a cold jet. J. Sound Vib. **64**(1), 73–83 (1979)
43. Panda, J., Seasholtz, R.G.: Experimental investigation of density fluctuations in high-speed jets and correlation with generated noise. J. Fluid Mech. **450**, 97–130 (2002)
44. Panda, J., Seasholtz, R.G., Elam, K.A.: Further progress in noise source identification in high-speed jets via causality principle. AIAA Paper 2003-3126 (2003)
45. Bogey, C., Bailly, C.: Investigation of sound sources in subsonic jets using causality methods on LES data. AIAA Paper 2005-2885 (2005)